Corrosion Science 53 (2011) 2344–2349

Contents lists available at ScienceDirect

Corrosion Science

journal homepage: www.elsevier.com/locate/corsci

Oxidation mechanism of a ZrB_2–SiC–ZrC ceramic heated through high frequency induction at 1600 °C

Wu Zhanjun [a], Wang Zhi [a,*], Qu Qiang [b], Shi Guodong [a]

[a] School of Aeronautics and Astronautics, Faculty of Vehicle Engineering and Mechanics, State Key Laboratory of Structural Analysis for Industrial Equipment, Dalian University of Technology, Dalian 116024, PR China
[b] China Academy of Launch Vehicle Technology R&D Centre, Beijing 100076, PR China

ARTICLE INFO

Article history:
Received 5 November 2010
Accepted 23 March 2011
Available online 29 March 2011

Keywords:
A. Ceramic matrix composites
B. SEM
C. Oxidation

ABSTRACT

In the present work, isothermal oxidation of a ZrB_2–(20 vol.%) SiC–(6 vol.%) ZrC (ZrB_2–SiC–ZrC) ceramic was carried out at a constant temperature of 1600 ± 15 °C in static air, and the microstructures of the surface and fractured surface of the oxidised specimen were observed using SEM. The change curve of weight change/unit area with increasing oxidation time was composed of four stages according to the increase in the oxidation time: initial, middle, middle-late and late. In the different stages, a mathematical model was formulated to interpret the oxidation behaviour of the ZrB_2–SiC–ZrC ceramic at high temperature.

1. Introduction

Zirconium diboride (ZrB_2) based ceramics have an extremely high melting point [1], high thermal and electrical conductivities [2], chemical inertness against molten metals [3] and good thermal shock resistance [4]. These unique mechanical and physical properties have never been achieved with other ceramic matrix composites. Increasing interest in the ZrB_2-based ceramics has stimulated research in the area during the past decade. Recently, ZrB_2-based ceramics have been considered for use in a variety of high temperature structural applications, such as rocket engines and thermal protection structures for leading-edge parts on hypersonic re-entry space vehicles [1–4]. This emerging attention is driven by demand for developing reusable hot-structures on space vehicles able to re-enter from low Earth orbit at relatively high speeds (on the order of 8 km/s) [5]. In contrast to traditional blunt capsules or shuttle-type vehicles, which are characterised by poor gliding capabilities and complex hot-structures, the future use of the ZrB_2-based ceramics opens up new avenues for the development of space planes with slender fuselage noses and sharp leading wing edges [6]. Components in high-flow environments, such as the leading edge of a hypersonic vehicle, are subjected to very high temperatures and require that geometric integrity be maintained during service [7]. The oxidation induced by high temperature is a major issue for the use of ZrB_2-based ceramics [8]. A history of studies on the oxidation of diborides has been given by Opeka et al. [9]. In the past 5 years, groups in the United States, Italy and China have investigated the oxidation behaviour of ZrB_2-based ceramics [8,10,11]. Fahrenholtz et al. [10] studied the microstructure of oxide scales on ZrB_2–SiC ceramics after oxidation at temperatures of up to 1500 °C. They reported that the typical scale was composed of three layers: (1) a SiO_2-rich glassy layer; (2) a thin ZrO_2–SiO_2 layer; (3) a SiC-depleted layer. These layered structures have been analysed with the aid of a thermodynamic model involving volatility diagrams for ZrB_2 and SiC [12]. Great efforts have been devoted to understanding the oxidation behaviour of ZrB_2-based ceramics, and a significant amount of progress has been made. Until now, understanding of the oxidation behaviour of ZrB_2-based ceramics has been primarily qualitative [8–13]. For engineering design and applications, a quantitative model is needed that predicts oxidation kinetics. It is desirable to predict factors such as oxide layer thickness and weight change under a set of complex conditions of temperature.

In the present work, isothermal oxidation of a ZrB_2–(20 vol.%) SiC–(6 vol.%) ZrC (ZrB_2–SiC–ZrC) ceramic was carried out in static air at a constant temperature of 1600 ± 15 °C, and the microstructures of the surface and fractured surface of the oxidised specimen were observed by SEM. Automatic fitting of the weight change/unit area and oxidation time at different stages of the oxidation process was carried out with the OriginPro system. A mathematical model was formulated to interpret the oxidation behaviour of the ZrB_2–SiC–ZrC ceramic at a temperature of 1600 °C.

2. Experimental

The preparation of a ZrB_2–(20 vol.%) SiC–(6 vol.%) ZrC (ZrB_2–SiC–ZrC) ceramic has been described elsewhere [14]. The bulk den-

* Corresponding author. Tel./fax: +86 411 84706791.
E-mail address: wzdlut@dlut.edu.cn (W. Zhi).

0010-938X/$ - see front matter © 2011 Elsevier Ltd. All rights reserved.
doi:10.1016/j.corsci.2011.03.024

sity of the ZrB_2–SiC–ZrC ceramic was measured using Archimedes' technique with deionised water as the immersing medium. The relative density was determined by dividing the bulk density by the theoretical density. The high frequency induction device had a power of 30 kW and was used to determine the oxidation behaviour of the ZrB_2–SiC–ZrC ceramic. Specimens for the analysis were $3 \times 4 \times 36$ mm. Each specimen was fixed in porous zirconia and the temperature of the specimen centre was measured with a multi-wavelength pyrometer with a measurement range of 1000–2500 °C. Isothermal oxidation of the specimens was carried out in static air at a constant temperature of 1600 ± 15 °C. The mass of the specimen was determined on an electronic balance; its accuracy was ±0.1 mg. The weight change/unit area (w) of the specimen was calculated by:

$$w = \frac{m_t - m_0}{A} \quad (1)$$

where m_0 and m_t are the weight of the specimen before and after an oxidation time of t s, respectively, and A is the surface area of the specimen. Microstructural observations of the specimen were carried out by scanning electron microscopy (SEM, FEI Sirion, Holland), along with energy dispersive spectroscopy (EDS, EDAX, Inc.) for chemical analysis.

3. Results and discussion

A typical SEM micrograph of the polished surface of the ZrB_2–SiC–ZrC ceramic is shown in Fig. 1. EDS analysis (not shown here) showed that the microstructure of the ZrB_2–SiC–ZrC ceramic was characterised by grey ZrB_2, dark SiC and light ZrC. The theoretical density of the ZrB_2–SiC–ZrC ceramic was calculated according to the rule of mixtures based on densities of 6.09, 3.21 and 6.44 g/cm^3 for ZrB_2, SiC and ZrC, respectively [14,15]. The theoretical density of ZrB_2 containing 20 vol.% SiC plus 6 vol.% ZrC was calculated to be 5.54 g/cm^3. Based on this bulk density, the relative density of the ZrB_2–SiC–ZrC ceramic was calculated to be >97.5%, which is higher than 95% of the ZrB_2–SiC ceramics produced by reactive hot-pressing at a temperature of 1400 °C [16]. The higher relative density obtained was due to the higher temperature.

The predominant phases for the ZrB_2–SiC–ZrC ceramic were ZrB_2, SiC and ZrC, and the total amount of various impurities was less than 1%. Consequently, the effect of impurities on the oxidation behaviour of the ZrB_2–SiC–ZrC ceramic was not considered in the present work. The surface of the specimen was oxidised when the specimen was exposed to high temperature air [8–13]. For example, ZrC is oxidised to ZrO_2 and CO_2 at temperatures above 380 °C; ZrB_2 is oxidised to ZrO_2 and B_2O_3 above 650 °C; and SiC is oxidised to SiO_2 and CO_2 above 900 °C. Therefore, ZrO_2 and SiO_2 can be formed on the surface of the specimen during heating. The main reactions expected are described as follows:

$$ZrC(s) + 2O_2 \rightarrow ZrO_2(s) + CO_2(g) \quad (2)$$

$$ZrB_2(s) + 5/2O_2 \rightarrow ZrO_2(s) + B_2O_3(g) \quad (3)$$

$$SiC(s) + 2O_2 \rightarrow SiO_2(l) + CO_2(g) \quad (4)$$

$$SiO_2(l) + B_2O_3(l) \rightarrow SiO_2 \cdot B_2O_3(l) \quad (5)$$

Fig. 2 shows SEM micrographs of the surface and fractured surface of the specimen oxidised at 1600 °C for 2 min. EDS analysis showed that the ZrB_2 and ZrC particles on the surface of the specimen were oxidised to a white ZrO_2 phase, which was partially covered with a thin SiO_2-rich layer, as shown in Fig. 2A. This SiO_2-rich layer was expected to contain some B_2O_3 during the heating at 1600 °C from either incomplete evaporation of the B_2O_3 or the continued production of B_2O_3 beneath the outer layer [10]. The fractured surface showed a clear interface and the thickness of the oxide layer was measured by SEM to be 12 μm, as shown in Fig. 2B. No poreS in the oxide layer were observed, which was attributed to both the short oxidation time and volume expansion based on density calculations conversion of the ZrB_2, ZrC and SiC to ZrO_2 and SiO_2.

The SEM micrographs of the surface and fractured surface of the specimen oxidised for 10 min are shown in Fig. 3. The surface was completely covered with a dark glass layer, and EDS analysis confirmed that the surface of the specimen mainly was composed of silicon and oxygen, indicating the surface was a SiO_2-rich layer. Furthermore, a small quantity of zirconium was measured by EDS in the oxide layer, which revealed that a partial ZrO_2 phase was covered by the thin SiO_2-rich layer. The thickness of the oxide layer was measured by SEM to be 15 μm, as shown in Fig. 3B. Compared with the fractured surface of the specimen oxidised for 2 min, obvious pores appeared in the fractured surface of the oxide layer due to active oxidation of the SiC phase, as shown in chemical Eq. (6) [12].

$$SiC(s) + O_2 \rightarrow SiO(g) + CO(g) \quad (6)$$

The formation of a porous microstructure resulted from the active oxidation of SiC particles, as has been noted by several researchers, and a thermodynamic model has been developed to explain the formation of a SiC-depleted layer during the oxidation of ZrB_2–SiC ceramics in air at 1500–1800 °C [12,17]. The active oxidation of SiC particles at low oxygen potentials and high temperatures results in the formation of gaseous SiO that can readily escape through the outer layer [18]. However, the pores that act as escape vents were not observed on the surface of the specimen, which was ascribed to that the pores being sealed by a SiO_2-rich layer and/or much smaller pores.

Fig. 4A shows a SEM micrograph of the surface of the specimen oxidised for 25 min. The surface was completely covered with a dark SiO_2-rich layer, and no white ZrO_2 phase was observed, revealing that the thickness of the SiO_2-rich layer increased as the oxidation time increased. Furthermore, obvious pores were observed under high magnification, as shown in the inset in Fig. 4A. These pores could act as diffusion channels for gaseous products to the outer layer and oxygen into the substrate. A SEM micrograph of the fractured surface of the specimen oxidised for 25 min is shown in Fig. 4B, where the thickness of the oxide layer was measured to be 28 μm. Compared with the fractured surface of the specimens oxidised for 2 and 10 min, the amount of pores in the oxide layer increased with increasing oxidation time. Furthermore, the increase in both the thickness of the oxide layer and the amount of the SiO_2-rich glass in the oxide layer with increasing

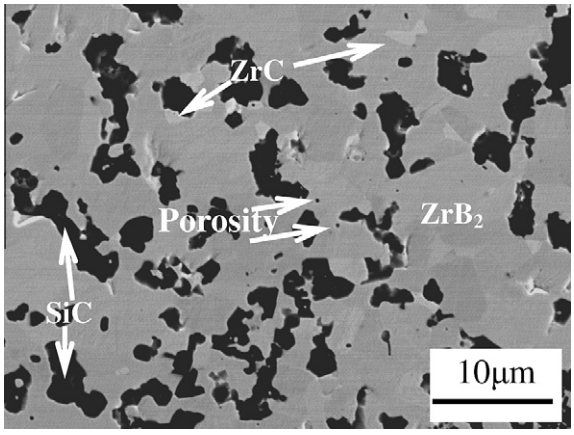

Fig. 1. Typical SEM micrograph of the polished surface of the ZrB_2–SiC–ZrC ceramic.

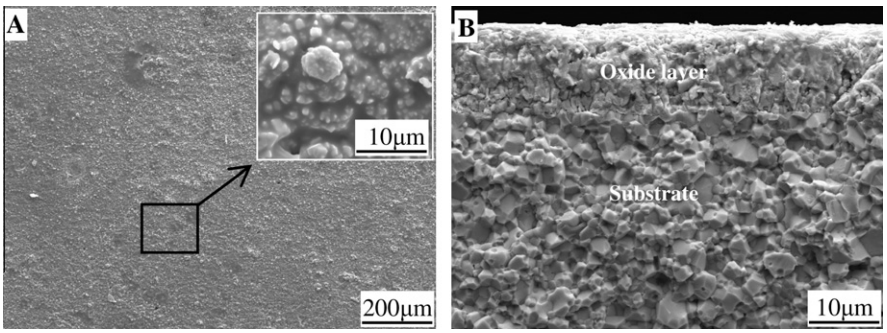

Fig. 2. SEM micrographs of the surface (A) and fractured surface (B) of the specimen oxidised at 1600 °C for 2 min.

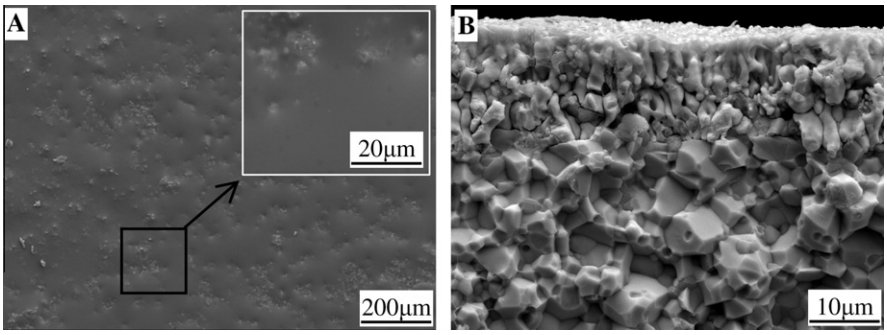

Fig. 3. SEM micrographs of the surface (A) and fractured surface (B) of the specimen oxidised at 1600 °C for 10 min.

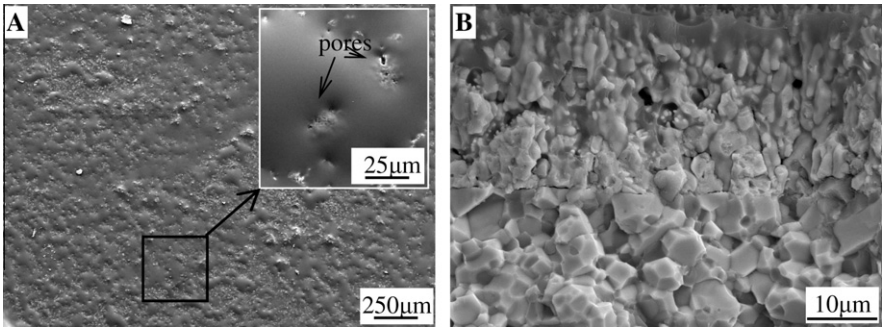

Fig. 4. SEM micrographs of the surface (A) and fractured surface (B) of the specimen oxidised at 1600 °C for 25 min.

oxidation time was attributed to both an increase in the oxidation time and diffusion of the SiO_2-rich glass into the pores.

A SEM micrograph of the surface of the specimen oxidised for 40 min is shown in Fig. 5A. The surface was completely covered with a dark SiO_2-rich layer, although this layer cracked due to volume shrinkage during specimen cooling. The formation of the large bubbles was attributed to the escape of gaseous products inside the outer glass layer [17]. The bubbles tended to burst when the vapour pressure of the bubbles exceeded the sum of the ambient pressure and the tensile force of the oxide layer, which resulted in the presence of pores on the surface of the oxidised specimen. Fig. 5B shows a SEM micrograph of the fractured surface of the specimen oxidised for 40 min, where the thickness of the oxide layer was measured to be 40 μm. The increase in the thickness of the oxide layer was attributed to the increase in the oxidation time and the presence of pores. Furthermore, the amount of pores increased due to further active oxidation of the SiC phase.

The change curve of weight change/unit area with increasing oxidation time was recorded and is shown in Fig. 6. The change curve of weight change/unit area with increasing oxidation time was paralinear, with an initial parabolic-like oxidation process transitioning to linear, likely due to volatility-driven mass loss [18–20]. Automatic fitting of the weight change/unit area and the oxidation time over the whole oxidation process was carried out with the OriginPro system. If the change curve was set to a form with an initial parabolic-like oxidation process transitioning to linear, a large deviation between the fitting curve and the data occurred. Therefore, the piecewise fitting was completed, and the fitted curve and data were in good agreement. The change curve of weight change/unit area with increasing oxidation time was composed of four stages, an initial stage, middle stage, middle-late stage and late stage. According to the kinetics of the gas–solid phase reaction [21–24], the oxidation process of polycrystalline materials is generally composed of two stages, namely (a) the oxygen molecules in the gas phase diffuse through the gas boundary layer to the reaction interface, and (b) the oxygen molecules diffuse through the oxide layer to the reaction interface. The curve of weight change/unit area with increasing oxidation time was approximately composed of four stages, which revealed the complicated oxidation process of the ZrB_2–SiC–ZrC ceramic because

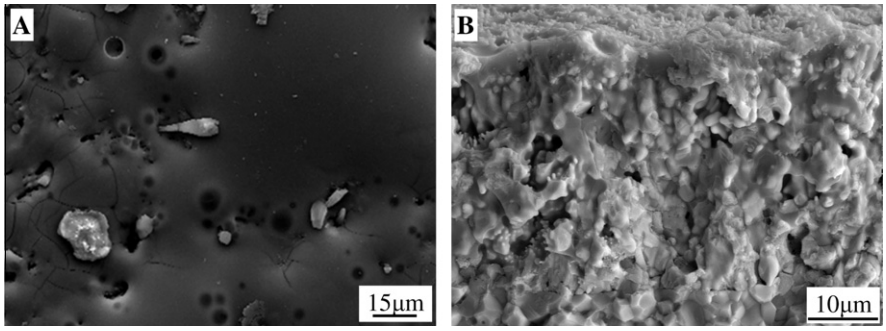

Fig. 5. SEM micrographs of the surface (A) and fractured surface (B) of the specimen oxidised at 1600 °C for 40 min.

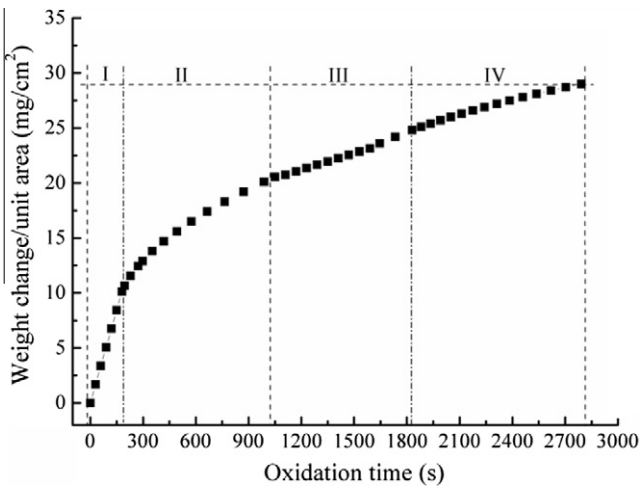

Fig. 6. The change curve of weight change/unit area with increasing oxidation time.

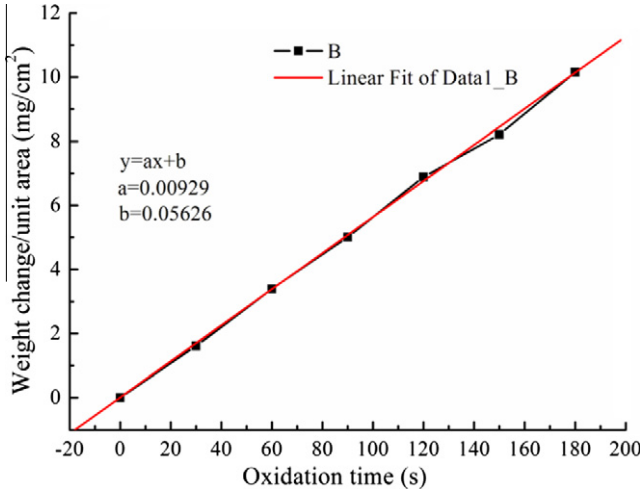

Fig. 7. The change curve of weight change/unit area with increasing oxidation time in the initial stage of the oxidation period.

multiple processes going on at once with oxide formation and mass loss via volatilisation of gaseous products, such as B_2O_3 and SiO [18–20].

To further investigate the oxidation mechanism of the ZrB_2–SiC–ZrC ceramic, automatic fitting of the weight change/unit area and the oxidation time in the initial stage of the oxidation process was carried out with the OriginPro system, as shown in Fig. 7. This fit indicated that the weight change/unit area linearly increased as the oxidation time increased. In the initial stage, the oxygen molecules in air were directly diffused by Van der Waals forces to the reaction interface, where they reacted with ZrB_2, SiC and ZrC at the surface of the specimen to produce oxides. The chemisorption nuclei formed on the surface of the specimen and the weight change/unit area due to oxidation was controlled by the chemical reaction rate. The linear increase in the weight change/unit area with increasing oxidation time indicated that the continuous SiO_2-rich layer on the surface of the specimen did not form in 200 s.

Automatic fitting of the weight change/unit area and the oxidation time in the middle stage of the oxidation process was carried out with the OriginPro system, as shown in Fig. 8, which showed that the weight change/unit area increased as the oxidation time increased in a parabolic fashion. The parabolic oxidation kinetics of the ZrB_2–SiC–ZrC ceramic could be explained by solid-state diffusion [25]. The continuous SiO_2-rich layer separated the unaffected substrate from the oxygen gas. The oxidation reaction could proceed only with the solid-state diffusion of the oxygen through the previously formed SiO_2-rich layer. Based on Fick's first law [26], the diffusion flux, J, of oxygen through the oxide layer can be defined as:

$$J = -D_0 A \frac{\partial C}{\partial x} \tag{7}$$

$$J \cong -D_0 A \frac{\Delta C}{x} \tag{8}$$

where A is the surface area of the specimen, ΔC is the concentration difference between the gas/oxide layer interface and the oxide

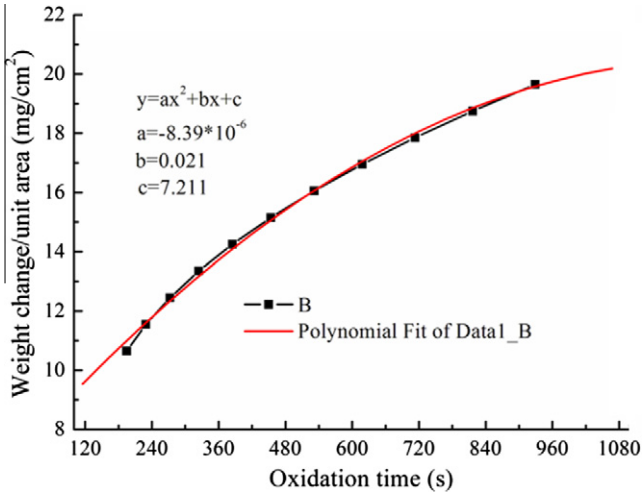

Fig. 8. The change curve of weight change/unit area with increasing oxidation time in the middle stage of the oxidation period.

layer/substrate interface and x is the thickness of the oxide layer. After the formation of a continuous SiO_2-rich layer a steady state was obtained and the diffusion flux, J, of oxygen through the oxide layer was equal to the quantity of oxygen consumed by oxide layer growth in unit time dt:

$$-D_0 A\frac{\Delta C}{x} = Al_0\frac{dx}{dt} \tag{9}$$

where dx is the thickness of the oxide layer growth and l_0 is the quantity of oxygen consumed by oxide layer growth. To integrate Eq. (9), the thickness of the oxide layer x was obtained as:

$$X^2 = \frac{2\Delta C D_0}{l_0}t \tag{10}$$

where ΔC, D_0 and l_0 in steady state are constants. Eq. (10) can thus be transformed as follows:

$$x^2 = kt \tag{11}$$

Based on theoretical derivations and experimental results, the oxidation reaction of the ZrB_2–SiC–ZrC ceramic in the middle stage was mainly controlled by the diffusion rate of oxygen through the SiO_2-rich layer because the oxidation kinetics obeyed a parabolic law, which was attributed to the formation of a continuous SiO_2-rich layer on the surface of the specimen.

Automatic fitting of the weight change/unit area and the oxidation time in the middle-late stage of the oxidation process was carried out with the OriginPro system as shown in Fig. 9. The fit indicated that the weight change/unit area linearly increased with increasing oxidation time, which was attributed to the presence of a significant number of pores. These pores allowed the weight change/unit area due to oxidation to be controlled by the chemical reaction rate instead of by the diffusion rate of oxygen through the SiO_2-rich layer. However, the oxidation rate (0.00495) in the middle-late stage of the oxidation process was less than that (0.00929) in the initial stage of the oxidation process, which was attributed to the area of the pores in the middle-late stage being less than the uncovered surface of the specimen in the initial stage of the oxidation process.

Automatic fitting of the weight change/unit area and the oxidation time in the late stage of the oxidation process is shown in Fig. 10. The weight change/unit area with increasing oxidation time followed a biquadratic law. It is generally believed that the particle transfer process in the oxide layer was controlled by both lattice diffusion and grain boundary diffusion. The ratio of the two kinds of diffusion changed with the changing microstructure and grain size of the oxides on the surface of the specimen. Assuming that the effective diffusion coefficient, D, was determined by the lattice diffusion coefficient, D_l, and the grain boundary diffusion, D_g:

$$D = D_l(1-f) + D_g f \tag{12}$$

where f is the ratio of the grain boundary to all of the diffusion points. Thus, at oxidation time t, the ratio of the grain boundary to unit area is:

$$f_t = \frac{2d}{(a_0^2+kt)^{1/2}} \tag{13}$$

where d is the width of the grain boundary, a_0 is the initial value of the grain length and k is a constant. The oxidation rate was derived according to the effective diffusion coefficient, D, as follows:

$$\frac{dx}{dt} = vD\frac{\Delta c}{x} \tag{14}$$

where x is the thickness of the oxide layer, t is the oxidation time, v is the volume of the oxide formed by each atom and Δc is the differential concentration of the oxygen in the oxide layer. Substituting Eqs. (12) and (13) into Eq. (14) provides:

$$2x\frac{dx}{dt} = 2vD_l\Delta c\left[1+\frac{D_g}{D_l}\times\frac{2d}{(a_0^2+kt)^{1/2}}\right] \tag{15}$$

When the specimen was oxidised, the density of the grain boundary observably increased, namely, $D_g >> D_l$. The main oxygen diffusion in the oxide layer was the lattice diffusion, and the change in the width of the grain boundary, d, with increasing oxidation time was neglected. Eq. (15) is thus transformed as follows:

$$2x\frac{dx}{dt} = 2vD_l\Delta c\frac{2dD_g}{(a_0^2+kt)^{1/2}} \tag{16}$$

Eq. (16) is then integrated:

$$X^2 = 8vdD_l\Delta c\frac{1}{k_0}(a_0^2+kt)^{1/2} \tag{17}$$

Assuming $k = 8vdD_b\Delta ck^{-1}$, simplified Eq. (17) is given as:

$$x^2 = k(a_0^2+kt)^{1/2} \tag{18}$$

Considering the initial condition, $t = 0$ and $x = 0$, Eq. (18) is thus transformed as follows:

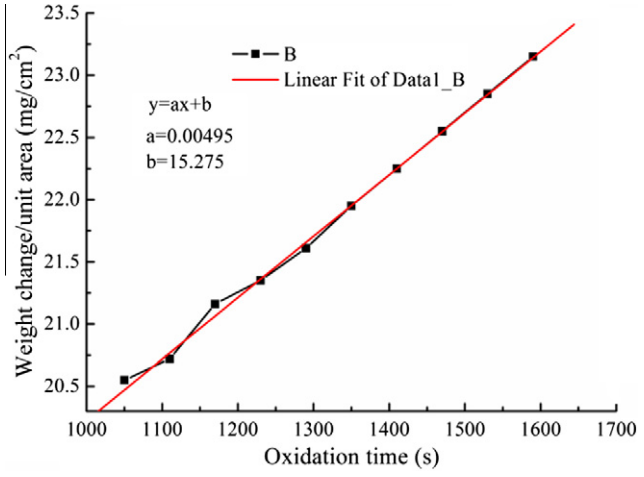

Fig. 9. The change curve of the weight change/unit area with increasing oxidation time in the middle-late stage of the oxidation period.

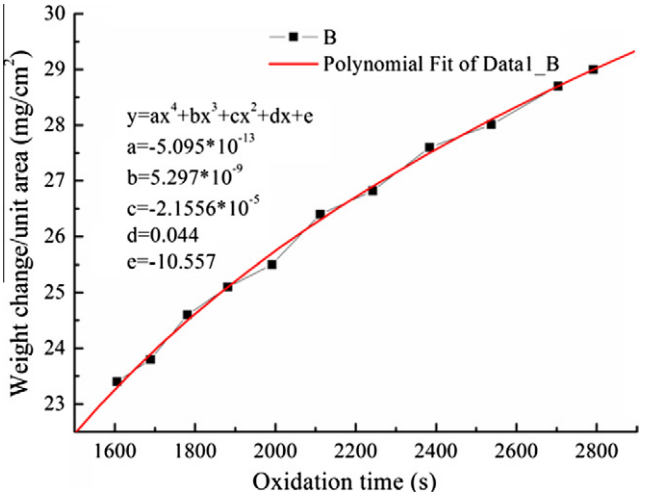

Fig. 10. The change curve of the weight change/unit area with increasing oxidation time in the late stage of the oxidation period.

$$x^4 = k_p^t + b \quad (19)$$

The growth of the oxide layer was controlled by lattice diffusion based on the classical Wagner's theory with a parabolic law ($x^2 = kt$) [27]. Compared with Wagner's theory, the obvious difference in oxidation kinetics of the ZrB_2–SiC–ZrC ceramic was attributed to the presence of the flaws in the oxide layer, such as the pores as shown in Fig. 5B.

The weight change/unit area with increasing oxidation time was controlled by the oxidation temperature and time as well as the surface morphology, particularly pores. Further work is continuing to investigate the oxidation mechanism of a ZrB_2–SiC–ZrC ceramic heated for longer times and under more complex conditions of temperature.

4. Conclusions

In the present work, isothermal oxidation of the ZrB_2–(20 vol.%) SiC–(6 vol.%) ZrC (ZrB_2–SiC–ZrC) ceramic was carried out in static air at 1600 ± 15 °C. The surface of the specimen was oxidised for 2 min to a white ZrO_2 phase, which was partially covered with a thin SiO_2-rich layer. The thickness of the oxide layer increased as the oxidation time increased up to 40 min. Additionally, the amount of pores in the oxide layer increased as the oxidation time increased up to 40 min. The change curve of weight change/unit area with increasing oxidation time was composed of four stages according to the increase in oxidation time: initial, middle, middle-late and late. In the initial stage, the chemisorption nuclei formed on the surface of the specimen and the weight change/unit area due to oxidation were controlled by the chemical reaction rate. The linear increase in the weight change/unit area with increasing oxidation time indicated that the continuous SiO_2-rich layer on the surface of the specimen did not form in 200 s. The oxidation reaction of the ZrB_2–SiC–ZrC ceramic in the middle stage was mainly controlled by the diffusion rate of oxygen through the continuous SiO_2-rich layer on the surface of the specimen. The presence of many pores resulted in the weight change/unit area in the middle-late stage being controlled by the chemical reaction rate instead of by the diffusion rate of oxygen through the SiO_2-rich layer. The weight change/unit area with increasing oxidation time followed a biquadratic law in the late stage, which was confirmed by theoretical derivations.

Acknowledgements

This work was supported by the China Postdoctoral Science Foundation Funded Project (20100481220), and Fundamental Research Funds for the Central Universities (3014-852001 and DUT10ZDG05) and the National Natural Science Foundation of China (51002019 and 91016024).

References

[1] F. Monteverde, Corros. Sci. 47 (2005) 2020–2033.
[2] S.B. Zhou, W.J. Li, P. Hu, C.Q. Hong, L. Weng, Corros. Sci. 51 (2009) 2071–2079.
[3] S.F. Tang, J.Y. Deng, S.J. Wang, W.C. Liu, Corros. Sci. 51 (2009) 54–61.
[4] P. Hu, G.L. Wang, Z. Wang, Corros. Sci. 51 (2009) 2724–2732.
[5] F. R. Savino. Monteverde, R. Savino, J. Eur. Ceram. Soc. 27 (2007) 4705–4797.
[6] D. Gao, Y. Zhang, J.Y. Fu, C.L. Xu, Y. Song, X.B. Shi, Corros. Sci. 52 (2010) 3203–3297.
[7] H.L. Wang, D.L. Chen, C.A. Wang, R. Zhang, D.N. Fang, Int. J. Refract. Met. Hard Mater. 27 (2009) 1024–1026.
[8] J.C. Han, P. Hu, X.H. Zhang, S.H. Meng, W.B. Han, Compos. Sci. Technol. 68 (2008) 706–799.
[9] M.M. Opeka, I.G. Talmy, E.J. Wuchina, J.A. Zaykoski, S.J. Causey, J. Eur. Ceram. Soc. 19 (1999) 2405–2414.
[10] A. Rezaie, W.G. Fahrenholtz, G.E. Hilmas, J. Eur. Ceram. Soc. 27 (2007) 2401–2495.
[11] F. Monteverde, A. Bellosi, J. Electrochem. Soc. 150 (11) (2003) B552–B559.
[12] W.G. Fahrenholtz, J. Am. Ceram. Soc. 90 (1) (2007) 143–148.
[13] S.N. Karlsdottir, J.W. Halloran, A.N. Grundy, J. Am. Ceram. Soc. 91 (1) (2008) 272–277.
[14] Q. Qu, J.C. Han, W.B. Han, X.H. Zhang, C.Q. Hong, Mater. Chem. Phys. 110 (2008) 216–221.
[15] X.H. Zhang, Q. Qu, J.C. Han, W.B. Han, C.Q. Hong, Scripta Mater. 59 (2008) 753–756.
[16] Y. Zhao, L.J. Wang, G.J. Zhang, W. Jiang, L.D. Chen, Int. J. Refract. Metal. Hard. Mater. 27 (2009) 177–180.
[17] J.C. Han, P. Hu, X.H. Zhang, S.H. Meng, Scripta Mater. 57 (2007) 825–828.
[18] E.J. Opila, R.E. Hann, J. Am. Ceram. Soc. 80 (1) (1997) 197–205.
[19] E.J. Opila, J. Am. Ceram. Soc. 82 (3) (1999) 625–636.
[20] E.J. Opila, J.L. Smialek, R.C. Robinson, D.S. Fox, N.S. Jacobson, J. Am. Ceram. Soc. 82 (7) (1999) 1826–1834.
[21] A.G. Barea, P. Ollero, B. Leckner, Chem. Eng. Sci. 62 (2007) 1477–1493.
[22] F. Gesmundo, B. Gleeson, Oxid. Metals. 44 (1-2) (1995) 211–237.
[23] D.J. Young, B. Gleeson, Corros. Sci. 44 (2002) 345–357.
[24] M.P. Brady, B. Gleeson, I.G. Wright, JOM 52 (2000) 16–21.
[25] N. Koga, H. Tanaka, Thermochim. Acta. 388 (2002) 41–61.
[26] C. Kohfahl, J. Greskowiak, A Pekdeger, Appl. Geochem. 22 (2007) 1–16.
[27] A. Korobkin, R. Guéret, Š. Malenica, J. Fluids Struct. 22 (2006) 404–493.